Select Applications of Carbon Nanotubes: Field-Emission Devices and Electromechanical Sensors

Amitesh Maiti[1]

Abstract: Atomistic modeling and simulations are becoming increasingly important in the design of new devices at the nanoscale. In particular, theoretical modeling of carbon nanotubes have provided useful insight and guidance to many experimental efforts. To this end, we report simulation results on the electronic, structural and transport properties for two different applications of carbon nanotube-based devices: (1) effect of adsorbates on field emission; and (2) effect of mechanical deformation on the electronic transport. The reported simulations are based on First Principles Density Functional Theory (DFT), classical molecular mechanics, and tight-binding transport based on the recursive Green's function formalism.

1 Introduction

Realistic application potentials and a steady growth of knowledge following the insightful work of a number of researchers have powered carbon nanotubes [Iijima (1991); Iijima Ichihashi, Ando (1992); Ebbesen, Ajayan (1992); Bethune et al. (1993); Iijima, Ichihashi (1993)] into a field of intense activity. A handful of commercial applications appear feasible in the not-too-distant future, including: Field Emission-based Flat Panel displays [W.A. de Heer, Charelain, Ugarte (1995); Rinzler, et al. (1995); Collins, Zettl (1996); Gulyaev et al. (1997); Fan et al. (1997); Küttel, Groenig, Emmenegger, Schlapbach (1998); Fransen, van Rooy, Kruit (1999); Iijima (1991)], novel semiconducting devices in microelectronics [Tans, Verchueren, Dekker (1998); de Heer Martel (2000)], hydrogen storage devices [Liu, et al. (1999)], structural reinforcement agents [Wong et al. (1997)], chemical sensors [Dai (2000)], and ultra-sensitive electromechanical sensors [Dai (2000)]. A number of important advances on the experimental front, including ability to manipulate matter at the nanoscale are pushing various prototype devices toward commercial reality. At the same time, the

simple atomic structure of carbon nanotubes and the high degree of structural purity are allowing accurate computer modeling using a variety of theoretical techniques. This paper is a review of our modeling endeavor in two application areas of carbon nanotubes: (1) effect of adsorbed molecules on the field emission from a metallic nanotube tip, and (2) effect of mechanical deformation on the electrical conductance of nanotubes.

2 Theoretical Techniques

2.1 First-Principles Density Functional Theory (DFT)

First-Principles methods of solving a many-electron Schrödinger equation can be broadly classified into two types: those based on the Hartree-Fock method, and those based on the Density Functional Theory (DFT). Due to better scaling with the number of electrons, DFT is quickly becoming the First-Principles technique of choice in technologically important problems. DFT is based on a theorem due to Hohenberg and Kohn (1964), which states that all ground state properties are functions of the total electronic charge density $\rho(r)$. The total energy of an electron gas can be formalistically written as a sum of the kinetic, potential (electrostatic), exchange and correlation energies. A practical implementation of this formalism into computer programs was made possible by the local density approximation (LDA) of Kohn and Sham (1965), which recast the many-electron problem into a problem of single electrons moving in an average field of the other electrons and ions. The basic formalism has stood the test of time, although important subsequent developments on gradient corrections to the LDA and the exchange-correlation functional have increased the accuracy of DFT significantly. There are several different DFT codes available commercially, differing primarily in the choice of the basis functions in which the electronic wave functions are expanded, and the scheme of integration. For the work reported here, we used the DFT

[1] Accelrys Inc., 9685 Scranton Road, San Diego, CA 92121

code DMol[3][2] distributed by Accelrys Inc. In the present work, the electronic wave functions were expanded in a double-numeric polarized (DNP) basis set with a real-space cutoff of 4.0 Å. Such a cutoff reduces computational requirements without significantly sacrificing accuracy, as has been explicitly verified in this and many other numerical experiments. An all-electron calculation was carried out on a "medium" integration grid using a gradient-corrected exchange-correlation functional due to Perdew, Burke, and Ernzerhof (1996). A thermal smear of 0.01 Hartree was applied to obtain faster SCF convergence, without affecting the structure and energetics to any significant degree.

2.2 Classical Molecular Mechanics

Some of the applications discussed here involve somewhat long nanotube structures with several hundred to a few thousand atoms. Performing first-principles DFT calculations on systems of such size is prohibitively expensive, and often unnecessary. In such situations we used classical molecular mechanics (MM) with accurate interatomic potentials describing the C-C interactions. The MM engine used was the Open Force Field (OFF) available through Accelrys' Cerius[2] interface[3]. The interatomic C-C potential was described by the Universal Forcefield (UFF) [Rappe, et al. (1992)], which has previously been used to study the mechanical properties of carbon nanotubes [Yao, Lordi (1998)].

2.3 Transport modeling

Computing conductance through a narrow wire is always tricky because contact effects can often overshadow the intrinsic molecular conductance of the wire. However, under the assumption of ideal semi-infinite contacts, we computed the transmission and conductance using the recursive Green's function formalism [Datta (1997), Svizhenko, Anantrara, Govindan, Biegel, Venugopal (2002)] within the framework of a nearest-neighbor sp^3-tight-binding Hamiltonian in a non-orthogonal basis. The parameterization scheme explicitly accounts for effects of strain in the system through a bond-length-

dependence of the Hamiltonian and the overlap matrices H_{ij} and S_{ij}, as in Papaconstantopoulos, Mehl, Erwin, Pederson (1998). First, the retarded Green's function G^R of the whole nanotube was determined by solving the following equation:

$$(E \cdot S_{ij} - H_{ij} - \Sigma_{L,ij} - \Sigma_{R,ij})G^{R,jk} = \delta_i^k, \tag{1}$$

where $\Sigma_{L,R}$ are the retarded self-energies of the left and the right semi-infinite contacts. The transmission at each energy were then found[4] [Lohez, Lanco (1983)] from the equation:

$$T(E) = G^{R,ij}\Gamma_{L,jk}G^{A,kl}\Gamma_{R,li}, \tag{2}$$

where $\Gamma_{L,R} = i(\Sigma_{L,R}^R - \Sigma_{L,R}^A)$ are the couplings to the left and right leads. Finally, the total conductance of the tube was computed using the Landauer-Büttiker formula:

$$G = \frac{2e^2}{h} \int_{-\infty}^{\infty} T(E)(-\frac{\partial f_o}{\partial E})dE, \tag{3}$$

where $f_o(E)$ is the Fermi-Dirac function.

3 Application Examples

3.1 Effect of adsorbates on the field emission from the tip of a metallic nanotube

Of all the application areas that carbon nanotubes are potentially useful for, the one closest to commercial realization are field-emission-based flat panel displays. Nanotubes with length-to-width ratio as large as 10^5 have been synthesized and advanced fabrication methods have been devised for generating self-aligned or patterned nanotube films on glass [Ren, et al. (1998)] or silicon [Fan et al. (1999)] substrate. Prototype displays have already been demonstrated by several companies and academic research groups [Wang et al. (1998); Saito, Uemura, Hamaguchi (1998); Choi et al. (1999)]. One of the main concerns of a field-emission-based flat-panel display device is to reduce the operating voltage. One way

---

[2] See *http://www.accelrys.com/doc/life/insight2K/dmol/ 2_Theory.html#193994*
for details of DFT implementation in DMol[3]
http://www.accelrys.com/mstudio/dmol3.html
[3] Cerius[2] software. Accelrys Inc. San Diego, CA. *http://www.accelrys.com/doc /materials/cerius40/FFBSim/FF_SimulTOC.doc.html*

[4] In the Eqs (1-3), summation is performed over the repeating roman indices. The lower and upper indices denote covariant and contravariant components of a tensor.

to achieve this is to introduce adsorbates that might effectively lower the ionization potential (IP) and facilitate the extraction of electrons. An important experimental work in this regard was done at Motorola [Dean, von Allimen, Chalamala (1999)], which studied changes in field emission behavior in the presence of various gases, i.e., O_2, H_2 and water vapor. While O_2 and H_2 did not affect the field emission behavior appreciably, adsorbed water was found to significantly enhance the emission current. The effect of water on field emission current was more pronounced at low emission currents, and there was evidence of stability of water molecules on the nanotube tip at temperatures as high as 900 K. In addition, the enhancement in field emission current was found to be more pronounced with an increase in the amount of water vapor.

In order to understand the difference between H_2 and water on the field-emission properties of carbon nanotubes, we carried out first-principles electronic structure calculations using the DFT code DMol^3. The nanotube tip was represented by a C_{60} half capping a three-layer stem of a (5, 5) armchair tube, known to be metallic from simple electronic structure arguments. The dangling bonds at the stem end were not saturated with H because the difference in electronegativities between H and C introduces an artificial dipole moment in the nanotube[5] . A uniform external field E_{FE}, directed toward the tube from above, was chosen to represent the electric field close to the tube tip under field emission conditions. For all calculations a magnitude of E_{FE} = 1 eV/Å was used as a ballpark figure around which field emission is known to occur for these systems. In order to be consistent with the uniform field representation, the length of the nanotube tip was constrained to be of the order of the tube diameter. The C-atoms at the stem end were frozen during all simulations in order to mimic the presence of a long stem in actual experiments.

Fig. 1 displays the minimum energy structures of a single hydrogen, a single water molecule, and a cluster of five water molecules adsorbed onto the nanotube tip. The H_2 molecule has two stable structures, *i.e. flat* or *upright* as indicated in Figs. 1(a) and 1(b). The water molecule in Fig. 1(c) has its dipole moment p along the nanotube axis, pointing down toward the tube, referred to below as *down water*. There is also an *up water* structure in which p points in the opposite direction. At E = 0 *up water* has nearly the same energy as *down water*, but under field emission conditions it becomes unstable and spontaneously flips into a *down water*. This structure is therefore, not considered further. Table 1 lists the binding energies of the various adsorbates, with the binding energy at E = 0 being defined as:

$$E_{\text{binding}}[E=0] = E_{\text{nanotube}}[E=0] + E_{\text{adsorbate}}[E=0]$$

$$- E_{\text{nanotube+adsorbate}}[E=0] \tag{4}$$

Therefore, positive binding denotes an exothermic process. *It is clear that binding for both H_2 and water is small at E=0, and that no adsorbate would be stable at the tube tip even at room temperature.* Orbital analysis showed that the highest occupied molecular orbital (HOMO), and several levels below HOMO, all belong to the nanotube and are delocalized for the metallic tip, resulting in some electron transfer to the adsorbates.

The above picture of weak interaction in zero fields drastically changes under field emission conditions when large electric fields E_{FE} are present at the tube tip. Since such a field is strongly focussed very close to the tube tip [Maiti, Brabec, Roland, Bernhole (1994)], a sensible definition of binding energy at E_{FE} is as follows:

$$E_{\text{binding}}[E=E_{FE}] = E_{\text{nanotube}}[E=E_{FE}]$$

$$+ E_{\text{adsorbate}}[E=0] - E_{\text{nanotube+adsorbate}}[E=E_{FE}] \tag{5}$$

---

[5] If the stem-end C-atoms of our 60-atom tip are H-saturated, each H-atom gains a positive charge of around 0.14 el, which leads to an intrinsic dipole moment of 3.7 a.u. in the nanotube. The resulting water-nanotube interaction is significant even at E = 0, *a result not consistent with experimental observations* (ref. [26]). In reality, the carbon nanotubes are much longer than the small tip we have been able to consider. A more realistic model would involve a very long tube ($\sim$ 1 micron or longer) with the end C-atoms at the stem-end being saturated with H (or perhaps a metal cluster from which the tube is growing catalytically). The net charge transfer to the whole tube would still be of the order of 1.4 el (0.14 el x 10 H atoms). However, most of this charge would reside close to the stem-end, i.e., far away from the tube tip where the adsorbate resides. The resulting adsorbate-nanotube interaction would, therefore, be small at E = 0. *Since we are limited to a small tip due to: (1) computational restrictions, and (2) consistency requirements with the uniform E-field model, we do *not* saturate the stem C-atoms with H.*
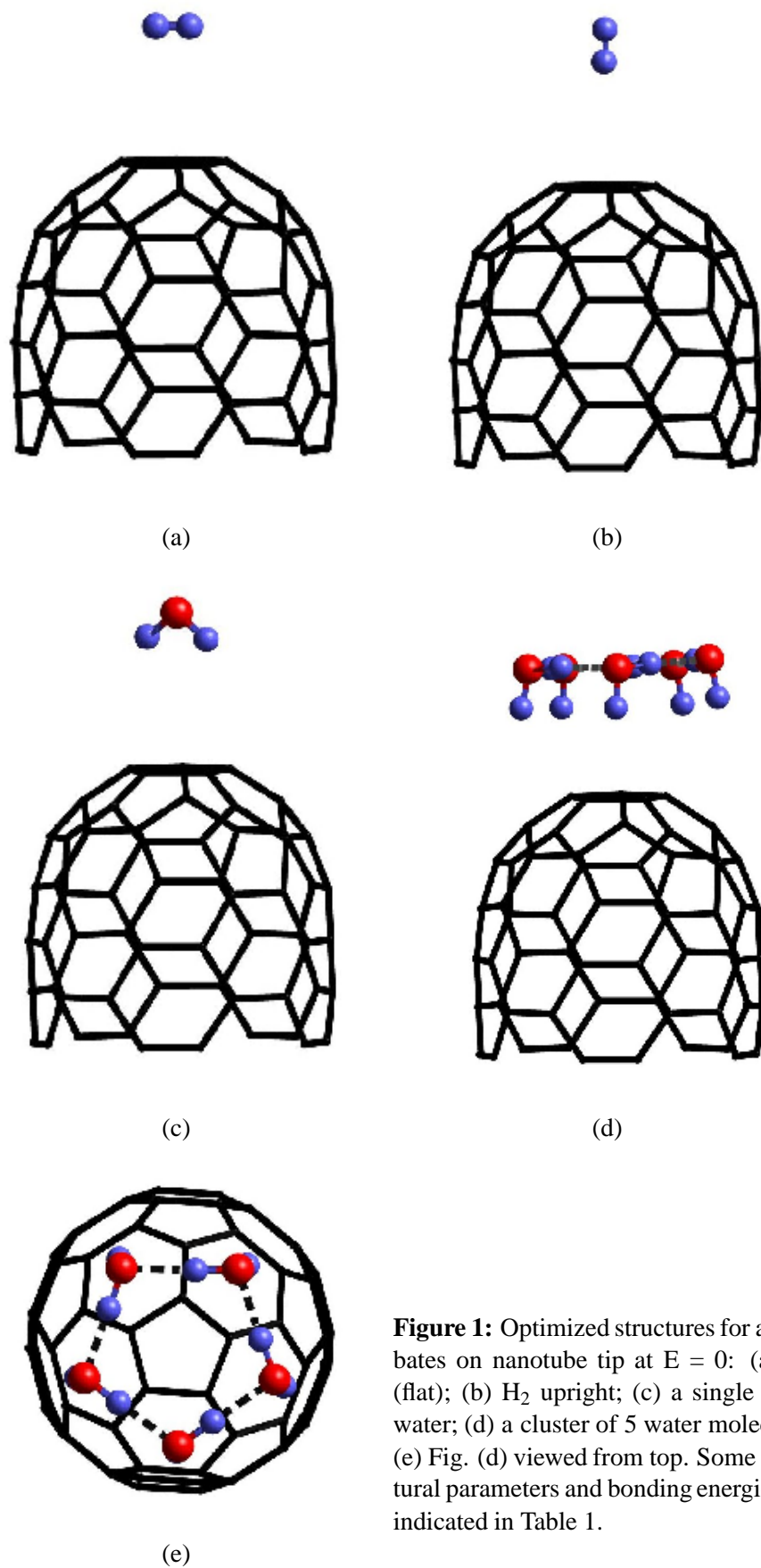
(a)

(b)

(c)

(d)

Figure 1: Optimized structures for adsorbates on nanotube tip at E = 0: (a) H_2 (flat); (b) H_2 upright; (c) a single down water; (d) a cluster of 5 water molecules; (e) Fig. (d) viewed from top. Some structural parameters and bonding energies are indicated in Table 1.

(e)

Table 1 : Binding energies, spatial separation, and charge transfer for optimized adsorbate structures on nanotube tip. $E_{binding}$ at E=0 and E=E_{FE} are computed according to Equations 4 and 5.

Adsorbates	$E_{binding}$ (kca/mol)		Distance of bottom Hl from tip (Å)		Charge transfer to adsorbate (el)	
	E = 0	E= E_{FE}	E = 0	E= E_{FE}	E = 0	E= E_{FE}
H_2 (flat)	0.0	1.1	3.02	3.03	- 0.020	- 0.054
H_2 (upright)	0.1	3.5	2.90	2.88	- 0.023	-0.071
1 Water	0.7	20.3	3.08	3.01	- 0.039	- 0.116
5 Water	—	65.0*, 101.4**	—	2.68	—	-0.340

* *w.r.t* a relaxed five-water complex at E = 0
** *w.r.t* five isolated water molecules at E = 0

$E_{binding}$ in equation (2) can be interpreted as the energy required to detach the adsorbate from the tube tip. This places the adsorbate away from the tip, where the field is negligible compared to E_{FE}. According to the above definition, the binding of the water molecule with the nanotube becomes more than 20 kcal/mol (at $E_{FE} = 1 \ eV/Å$), nearly the strength of a chemical bond. The H_2 molecule has a much weaker binding, more so in the flat configuration, and would not be stable on the tube tip even at room temperatures. This explains why they do not affect the field emission behavior from the tube tip.

In order to explore the effect of more than one water molecule at the nanotube tip, we considered a H-bonded cluster of five water molecules (Fig. 1(d, e)). The size 5 was chosen because of the fivefold symmetry of the nanotube tip about its axis, which made it easy to determine the global minimum of such a structure. As indicated in Table 1, the total binding energy of this complex to the nanotube is 65.0 kcal/mol with respect to an isolated five-water complex, and 101.4 kcal/mol with respect to five isolated water molecules. These numbers divided by 5 suggest that each water molecule has a net binding of $\sim$ 20.3 kcal/mol, of which about 13.0 kcal/mol is due to direct water-nanotube interaction and 7.3 kcal/mol arises out of H-bonding interactions among the water molecules themselves. Thus, the loss in individual water-nanotube binding (as compared to the case of a single water on nanotube) is exactly compensated by the gain in water-water binding. Thus, the formation of a water complex should not lower the temperature at which an individual water molecule in the cluster desorbs from the tip.

Structural changes are rather small even under large electrostatic forces at E = E_{FE}. In particular, the distance between the adsorbate and the nanotube changes by less than 0.07 Å, and the bond-lengths change by less than 0.01 Å. The most significant geometrical change is in the H-O-H angle in water, which decreases from 103.7^o in E = 0 to 98° on the tube tip at E_{FE} = 1 eV/Å. Such a change in angle leads to only a 0.02 a.u. increase in the dipole moment of water. It should also be noted that even at E_{FE}, the adsorbates are $\sim$ 3 Å above the tube tip, and the computed charge density in the middle of this separation is less than 0.004 el/Å^3. This is consistent with the binding being primarily electrostatic in nature. In fact a more detailed analysis of the dipole moment of the nanotube and the adsorbates in the presence and absence of electric field suggests that the nanotube gains a large dipole moment in the presence of E_{FE}, and this induced dipole interacts strongly with the intrinsic dipole moment of water. The water dipole also gains a significant energy from E_{FE} being parallelly aligned with the electric field.

Finally, we attempt an explanation of why water adsorption enhances field emission. To this end, we have computed the ionization potential for three systems at $E_{FE} = 1eV/Å$, i.e., nanotube, (nanotube + 1 adsorbed water), and (nanotube + 5 adsorbed water). The Ionization Potential is defined in a standard way, i.e. the energy difference between a system with a +1 charge (i.e. one less electron) and the original system with zero charge. The lower the IP, easier it is to extract an electron, and higher the expected Field emission current at a given operating voltage. In metallic nanotubes, the "hole" left by an emitted electron recombines almost instantaneously with an incoming electron from the stem side. Therefore, the structure with a +1 charge was frozen at the relaxed geometry for the neutrally charged system. Our results indicate that the presence of a single water molecule lowers the IP

by 0.1 eV and the presence of five water molecules lowers the IP by 0.6 eV, as compared with the isolated nanotube. In addition, we find that the position of the HOMO becomes unstable by 0.1 eV and 0.6 eV respectively in the presence of one water and the five-water cluster on the nanotube tip (at $E = E_{FE}$). This correlates perfectly with the corresponding lowering of the ionization potential. Thus, it appears that a polar adsorbate like water exerts an electrostatic field, which makes the HOMO unstable, thereby making it easier to extract electrons out of nanotube tips and enhancing the field-emission current [Maiti, Andzelm, Tanpipat, Von Allmen (2001)].

3.2 Carbon nanotubes as nano-electromechanical sensors (NEMS)

Interest in the application of carbon nanotubes as electromechanical sensors got a significant boost from the pioneering experiment of Tombler *et al.*[Tombler, et al. (2000)], in which the middle part of the segment of a metallic nanotube suspended over a trench was pushed with an AFM tip. Beyond a deformation angle of $\sim 10°$ the electrical conductance of the tube dropped by more than two orders of magnitude. The effect was found to be completely reversible, i.e., through repeated cycles of AFM-deformation and tip removal, the electrical conductance displayed a cyclical variation with constant amplitude.

The drop in conductance in the AFM-deformed tube was much higher than the computationally predicted values for tubes *bent* under mechanical duress. Such calculations, using both tight-binding [Nardelli, Bernholc (1999)] and semi-empirical Extended-Hückel type approaches [Rochefort, Avouris,Lesage, Salahub (1999)] concluded that even under large bending angles the reduction in electrical conductance was less than an order of magnitude. For AFM-deformed nanotubes, in contrast, O(N) tight-binding calculations [33] show that beyond a critical deformation several C-atoms close to the AFM tip become sp^3-coordinated. The sp^3 coordination ties up delocalized π-electrons into localized σ-states. This would naturally explain the large drop in electrical conductivity, as verified by explicit transport calculations.

In this work, we carried out a combination of first-principles DFT (DMol^3) and molecular mechanics (UFF) to investigate both forms of deformation, i.e., bending and AFM-deformation. Under either form of de-

formation bond reconstruction, if any, is likely to occur only in the highly deformed, non-straight part of the tube in the middle. This prompted us to use a DFT-based quantum mechanical description of the middle part of the tube ($\sim$ 100-150 atoms), while the long and essentially straight part away from the middle was described accurately using the Universal Forcefield (UFF).

Because of known difference in electronic response of zigzag and armchair tubes to mechanical deformation, we studied a (12, 0) zigzag and a (6, 6) armchair tubes, each consisting of 2400 atoms. For bending simulations, two halves of the tube were rotated by equal and opposite angles about an axis perpendicular to the tube and passing through the center of mass of the initial straight tube. At each end of the tube, a contact region defined by a unit cell plus one atomic ring (a total of 36 and 60 atoms for the armchair and the zigzag tube respectively) was then fixed and the whole tube relaxed with the UFF. The AFM tip was modeled by a 6-layer deep 15-atom Li-needle normal to the (100) direction, terminating in an atomically sharp tip. To simulate AFM-tip-deformation, the Li-needle was initially aimed at the center of a hexagon on the bottom-side of the middle part of tube. The Li-needle tip was then displaced by an amount δ toward the tube along the needle-axis, resulting in a deformation angle $\theta = tan^{-1}(2\delta/L)$, L being the unstretched length of the tube. The whole tube was then relaxed by UFF keeping the needle atoms and the end contact regions of the tube fixed. The contact region atoms were fixed in order to simulate an ideal undeformed semi-infinite carbon nanotube lead, and to ensure that all possible contact modes are coupled to the deformed part of the tube. Following the UFF relaxation, a cluster of 132 C-atoms for the (6, 6) and a cluster of 144 C-atoms for the (12, 0) were cut out from the middle of the tubes. These clusters, referred to below as the *QM clusters* (plus the 15 Li-tip atoms in tip-deformation simulations) were further relaxed with Accelrys' DFT-code DMol^3, with the end atoms of the cluster plus the Li-tip atoms fixed at their respective classical positions. In order to cut down on CPU requirements, the DFT calculations were performed using the Harris functional [Lin, Harris (1992); Li, Andzelm, Harris, Chaka(1995)] and the exchange-correlation potential due to Vosko, Wilk and Nusair (1980).

Fig. 2 displays the tip-deformed QM-cluster for the (6, 6) and the (12, 0) tubes at the highest deformation angle of 25° considered in these simulations. Even un-
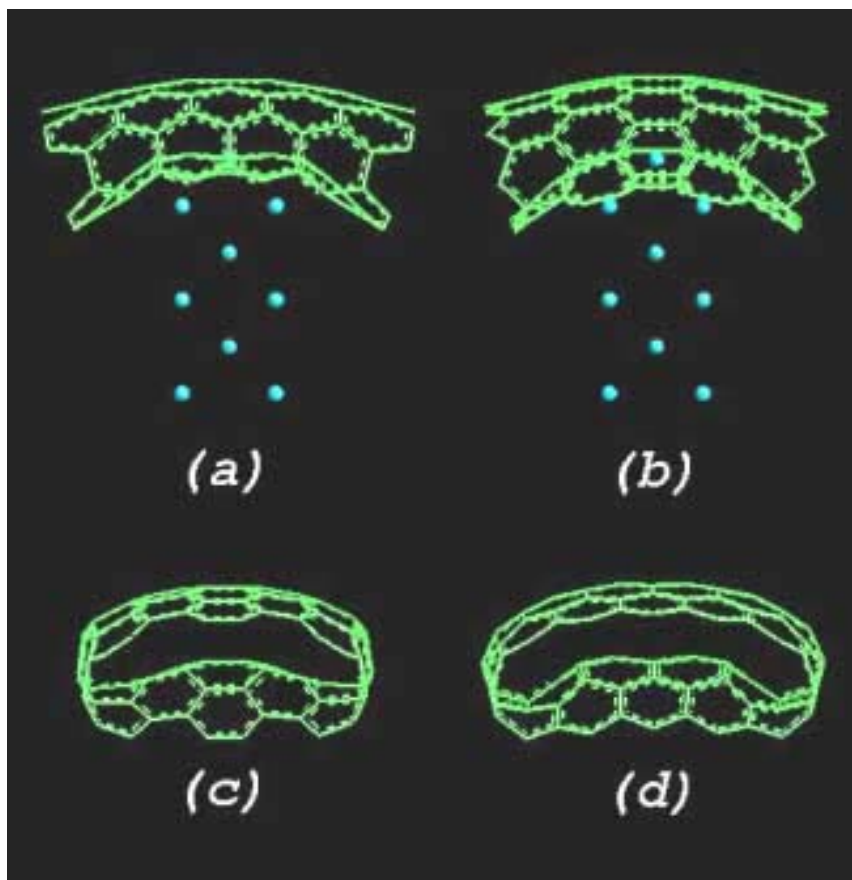
Figure 2 : DMol^3-relaxed Li-tip-deformed QM clusters for: (a) the (6, 6) armchair (132 C-atoms); and (b) the (12, 0) zigzag (144 C-atoms), in side views. The deformation angle is $25°$ for both tubes. Figs. (c) and (d) are respective views along the tube length, with the Li-tip hidden for clarity.

der such large deformations, there is no indication of sp^3 bonding, and the structure was very similar to what was observed for the (5, 5) tube in Maiti (2001). Although not explicitly shown here, results for *bending* also yield sp^2-coordinated all-hexagonal tubes, and the results were is good agreement with previously simulated results [Iijima, et al. (1996)]. The absence of sp^3 coordination is inferred based on an analysis of nearest neighbor distances of the atoms with the highest displacements, i.e., the ones on the top of the kink in a bent tube, and the ones closest to the Li-tip in a tip-deformed tube. Although for each of these atoms the three nearest neighbor C-C bonds are stretched to between 1.45-1.75 Å, the distance of the fourth neighbor, required to induce sp^3 coordination is greater than 2.2 Å for all tubes in our simulations. The main difference between a tip-deformed tube versus a bent tube is that there is an overall stretching in the former, whereas in the latter case there is no net stretching, as indicated schematically in Fig. 3. In the bending case,

the extra compressive strain on the bottom side of the tube is relieved through the formation of a *kink* beyond a critical bending angle.

Following structural relaxation of the nanotubes, we computed the transmission and conductance using the formalism outlined in section 2.3. Fig. 4 displays the computed room temperature conductance for the (6, 6) and the (12, 0) tubes as a function of bending and tip-deformation angles. The conductance remains essentially constant for the (6, 6) tube in either bending or tip-deformation simulations. However, for the (12, 0) tube the conductance drops by a factor of 1.9 under bending at $θ=40^o$, and much more significantly under tip deformation: by ~ 0.3 at 15°, two orders of magnitude at 20°, and 4 orders of magnitude at $θ=25°$.

To uncover the cause of conductance drop under tip deformation, we have performed electronic density of states (DOS) analysis for various parts of the tube. This anal-
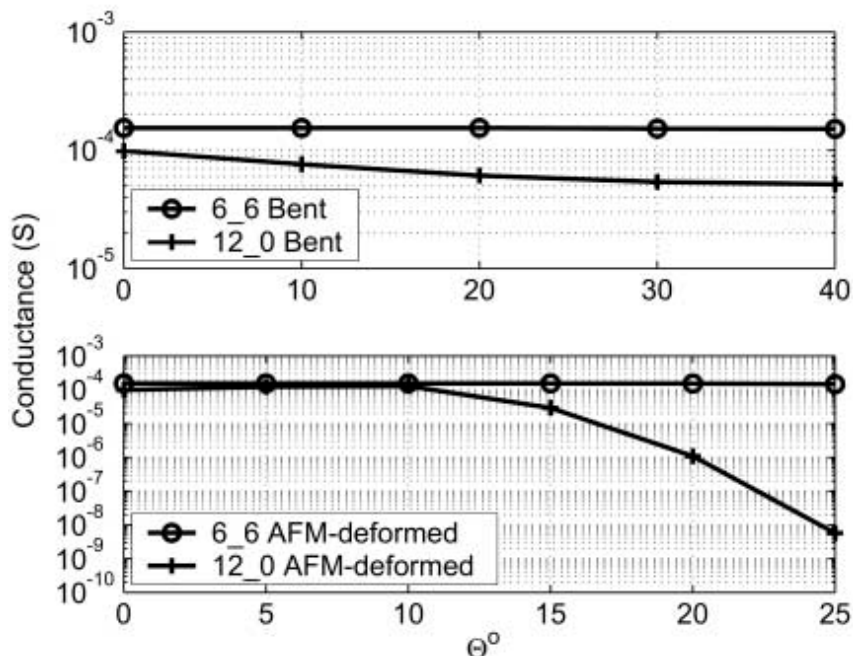
Figure 4 : Computed conductance (at T = 300K) for the (6, 6) and (12, 0) nanotubes as a function of: **(top)** bending; and **(bottom)** tip-deformation. Under 40° bending conductance of the zigzag tube drops by a factor of 1.9, while for the armchair tube it drops by only 1.01. Under 25° tip-deformation, conductance of the zigzag tube drops by 4 orders of magnitude, while for the armchair tube it drops only by a factor of 1.05.
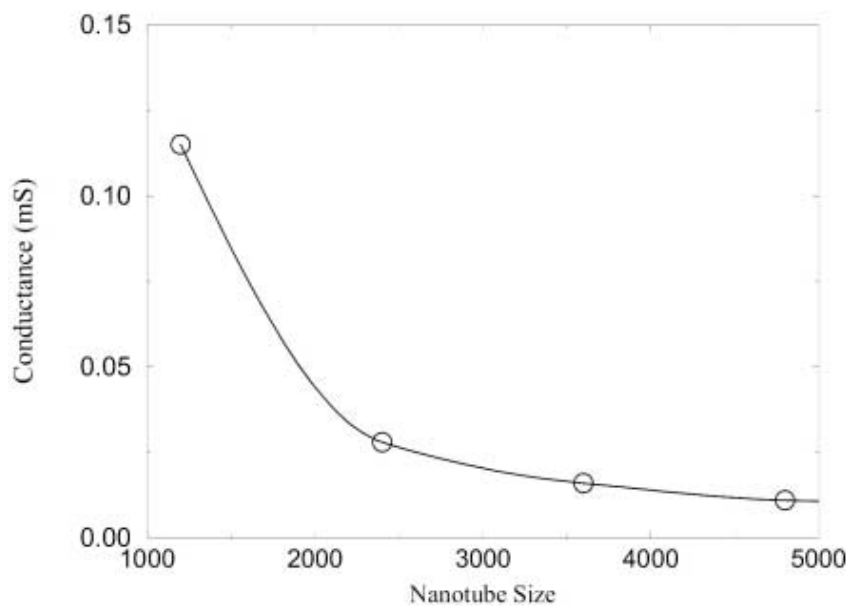

Figure 5 : Conductance (in milli-Siemens) for the (12, 0) nanotube as a function of the nanotube size at a constant tip-deformation angle of 15°. The saturation value for experimentally long tubes at this deformation angle is ~ 0.08 mS.
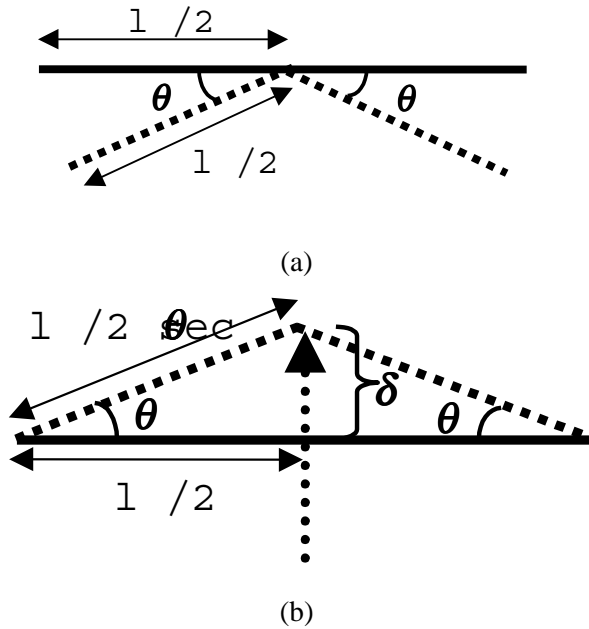
(a)

(b)

Figure 3 : Schematic diagrams representing: (a) bending; and (b) deformation with an AFM tip. The bent tube does not undergo an overall change in length, while the tip-deformed tube suffers a tensile strain. The tip-deformation angle θ is related to the tip displacement (δ) and non-deformed tube-length (l) by $\theta = tan^{-1}(2\delta/l)$.

ysis points to the fact that the drop occurs not only in the most highly deformed region in the middle, but also across the whole stretched (straight) section of the nanotube. This picture is consistent with the fact that the drop is much more significant in AFM-tip-deformed tubes where there is a net stretching. Interestingly, the fraction of the straight stretched part of the tube is small in shorter tubes (due to the presence of contact regions) than in longer tubes (with the same size for the contact region). This leads to a conductance drop as a function of increasing tube length, as indicated in Fig. 5. As a further exploration, we have also computed the drop in conductance in the (12, 0) tube as a function of a uniform stretching. The resulting drop in conductance compares remarkably well with the results for tube deformed with a Li-tip [39]. This has important implications for the application of nanotubes as electromechanical sensors: *given a metallic zigzag nanotube, one could induce a significant conductance drop simply upon uniform stretching.*

In order to explain the differences in conductance drops of the armchair (6, 6) and the zigzag (12, 0) tubes as a function of strain, we have analyzed the bandstructures of a metallic zigzag and an armchair nanotube under strain. The magnitude of the strain-induced bandgap decreases monotonically with increase in chiral angle [Maiti, Svizhenko, Anantram (2002); Heyd, Charlier, McRae (1997)], being maximum for a chiral angle of $0°$ (zigzag) and gradually reducing to zero at a chiral angle of $30°$ (armchair). An experiment as in Tombler, et al. (2000) is, thus, expected to show a decrease in conductance as the nanotube is deformed with an AFM tip, for all nanotubes except the armchair tube. The decrease in conductance should be large for the metallic zigzag nanotubes, and small for nanotubes with a chiral angle closer to armchair.

4 Future work

Both nanotube-based application areas discussed above, i.e., flat panel displays and nano-electromechanical sensors hold out promise for commercialization in the not-too-distant future. Further modeling and experimental work in these areas are, therefore, of great technological importance.

For the flat panel displays, one could possibly lower operating voltages even further by lowering the work function of the nanotube through suitable functional groups. Computing the IP in presence of a functional group should be straightforward, except for large functional groups on wider nanotubes, which makes the computation CPU-intensive. A bigger challenge is to compute the field-emission current itself. One would have to take recourse to some sort of a tunneling description, e.g., a Bardeen Transfer Hamiltonian formalism [Bardeen (1961)]. This would likely involve integration of a DFT code (like DMol^3) with an appropriate electronic transport code.

For the NEMS, there are also a lot of possibilities. Lowering conductance based on stretching of tubes is already an attractive idea and relevant experiments are soon expected to be underway. There could also be other forms of deformation. Recent calculations at NASA already suggest that in the case of torsional deformation, bandgaps open up for armchair tubes and not for zigzags, thus reversing the picture obtained in section III.2. There also have been experiments in several groups in which the deformed nanotubes are not suspended, but rather pushed against a fixed substrate. We are looking into such simulations as important differences are expected

due to different boundary conditions. Another area of interest is to study the effect of tip-nanotube interaction, in particular that of charge transfer, on the conductance properties.

References

Bardeen, J. (1961): *Phys. Rev. Lett.* **6**, 57.

Bethune, D. S.; et al. (1993): *Nature* **363**, 605.

Choi, Y. B.; et al. (1999): Appl. Phys. Lett. **75**, 3129.

Collins, P. G.; Zettl, A. (1996) *Appl. Phys. Lett.* 69, 1969

Dai, H. (2000): *Physics World*, June 2000, 43.

Datta, S. (1997): *Electronic Transport in Mesoscopic Systems*, Cambridge University Press.

Dean, K. A.; von Allmen, P.; Chalamala, B. R. (1999): textitJ. Vac. Sci. Technol. B **17**, 1959.

de Heer, W. A.; Chatelain, A.; Ugarte, D. (1995) *Science* **270**, 1179.

de Heer, W. A.; Martel, R. (2000): *Physics World*, June 2000, 49.

Ebbesen, T. W.; Ajayan, P. M. (1992): *Nature* **358**, 220.

Fan, S.; et al. (1997): *Science* **283**, 512.

Fan, S.; et al. (1999) *Science* **283**, 512.

Fransen, M. J.; van Rooy, Th. L.; Kruit, P. (1999): *Appl. Surf. Sci.* **146**, 312

Gulyaev, Y. V.; et al. (1997): *J. Vac. Sci. Technol.* B 15, 422.

Heyd, A.; Charlier, A.; McRae, E.; (1997): *Phys. Rev. B* **55**, 6820.

Hohenberg, P.; Kohn, W. (1964): *Phys. Rev. B* **136**, 864.

Iijima, S. (1991): *Nature* **354**, 56.

Iijima, S.; Brabec, C.; Maiti, A.; Bernholc, J. (1996): *J. Chem. Phys.* **104**, 2089.

Iijima, S.; Ichihashi, T. (1993): *Nature* **363**, 603.

Iijima, S.; Ichihashi, T.; Ando, Y. (1992): *Nature* **356**, 776.

Kohn, W.; Sham, L. J. (1965): *Phys. Rev. A* **140**, 1133.

Küttel, O.M.; Groenig, O.; Emmenegger, C.; Schlapbach, L. (1998): *Appl. Phys. Lett.* **73**, 2113.

Li, X. P.; Andzelm, J. W.; Harris, J.; Chaka, A. M. (1995): American Chemical Society, Anaheim Symposium.

Lin, Z. and Harris, J. (1992): *J. Phys.: Condens. Matter* **4**, 1055.

Liu, C.; et al. (1999): *Science* **286**, 1127.

Liu, L.;Jayanthi, C. S.; Dai, H. (2000): *Phys. Rev. Lett.* **84**, 4950.

Lohez, D.; Lanoo, M. (1983): *Phys. Rev. B* **27**, 5007.

Maiti, A. (2001): *Phys. Stat. Sol. B* **226**, 87.

Maiti, A.; Andzelm, J.; Tanpipat, N.; Von Allmen, P. (2001): *Phys. Rev. Lett.* **87**, 155502.

Maiti, A.; Brabec, C. J.; Roland, C.; Bernholc, J. (1994): *Phys. Rev. Lett.* **73**, 2468.

Maiti, A.; Svizhenko, A.; Anantram, M.P. (2002) *Phys. Rev. Lett.* **88**, 126805 (2002).

Nardelli, M.; Bernholc, J. (1999): *Phys. Rev. B* **60**, R16338.

Papaconstantopoulos, D. A.; Mehl, M. J.; Erwin, S. C.; Pederson, M. R. (1998): Tight-Binding Approach to Computational Materials Science, *MRS Proceedings* **491**, (Materials Research Society, Warrendale, PA.

Perdew, J. P.; Burke, K.; Ernzerhof, M. (1996): *Phys. Rev. Lett.* **77**, 3865.

Rappe, A. K.; Casewit, C. J.; Colwell, K. S.; Goddard, W. A.; Skiff, W. M. (1992): *J. Am. Chem. Soc.* **114**, 10024.

Ren et al. (1998) *Science* **282**, 1105.

Rinzler, A. G. et al. (1995): *Science* **269**, 1550.

Rochefort, A.; Avouris, P.; Lesage, F.; Salahub, D. (1999): *Phys. Rev. B* **60**, 13824.

Saito, Y.; Uemura, S.; Hamaguchi, K. (1999): *Jpn. J. Appl. Phys.*, Part 2, **37**, L346.

Svizhenko, A.; Anantram, M. P.; Govindan, T. R.; Biegel, B.; Venugopal, R. (2002): *J. Appl. Phys.* **91**, 2343.

Tans, S. J.; Verchueren, A. R. M.; Dekker, C. (1998) *Nature* **393**, 49.

Tombler et al. (2000): *Nature* **405**, 769.

Vosko, S. H.; Wilk, L.; Nusair, M. (1980): *Can. J. Phys.* **58**, 1200.

Wang, Q. H.; et al. (1998): *Appl. Phys. Lett.* **72**, 2912.

Wong; et al. (1997): *Science* **277**, 1971.

Yao, N.; Lordi, V. (1998) *J. Appl. Phys.* **84**, 1939.